COSMIC STRUCTURE FORMATION AT HIGH REDSHIFT

ILIAN T. ILIEV
Astronomy Centre, Department of Physics & Astronomy, Pevensey II Building, University of Sussex, Falmer, Brighton BN1 9QH, United Kingdom

KYUNGJIN AHN
Department of Earth Science Education, Chosun University, Gwangju 501-759, Korea

JUN KODA, PAUL R. SHAPIRO
Department of Astronomy, University of Texas, Austin, TX 78712-1083, U.S.A.

UE-LI PEN
Canadian Institute for Theoretical Astrophysics, University of Toronto, 60 St. George Street, Toronto, ON M5S 3H8, Canada

We present some preliminary results from a series of extremely large, high-resolution N-body simulations of the formation of early nonlinear structures. We find that the high-z halo mass function is inconsistent with the Sheth-Tormen mass function, which tends to over-estimate the abundance of rare halos. This discrepancy is in rough agreement with previous results based on smaller simulations. We also show that the number density of minihaloes is correlated with local matter density, albeit with a significant scatter that increases with redshift, as minihaloes become increasingly rare. The average correlation is in rough agreement with a simple analytical extended Press-Schechter model, but can differ by up to factor of 2 in some regimes.

1 Introduction

The properties of the first luminous objects in the universe remain a big enigma at present due to the scarcity of observational data. These objects, the first stars and galaxies, started forming very early, only about 100-200 million years after the Big Bang, and their ionizing radiation eventually completely reionized the intergalactic medium [1]. This complex process can be studied through numerical simulations and semi-analytical models. The former have the advantage of being able to describe complex situations and, in particular, the non-linearities of the cosmic structures, but are expensive to run and have limited dynamic range. The latter are much cheaper to run and thus allow studies of the full parameter space, but inevitably involve many approximations and simplifications. The distribution and properties of the low-mass halos which host the first stars is an important ingredient in any semi-analytical model of reionization. Such small-scale structure potentially has very different properties from larger structures we see at later times, as they probe a very different part of the initial power spectrum of density fluctuations. Therefore, it is important to check the validity of any models and fits to the halo mass function and bias in this new regime.

2 Simulations

The results we present in this work are based on series of very large N-body simulations, as summarized in Table 1. They follow between 1728^3 (5.2 billion) and 5488^3 (165 billion) particles (the latter at present is the largest cosmic structure formation simulation ever performed) in a wide range of box sizes from $2/h$ Mpc up to $3.2/h$ Gpc. Spatial resolution ranges from 50 pc/h to 40 kpc/h, while the particle masses range from 100 $M_\odot$ up to $\sim 6 \times 10^{10}$, which yields minimum resolved halo masses (with 20 particles) between $2 \times 10^3 M_\odot$ and $10^{12} M_\odot$. The simulations were performed with the code CubeP^{3}M[a] [2].

Table 1: N-body simulation parameters. Background cosmology is based on the WMAP 5-year results.

boxsize	N_{part}	mesh	spatial resolution	$m_{particle}$	$M_{halo,min}$
$2\,h^{-1}$Mpc	2048^3	4096^3	$48.8\,h^{-1}$pc	$99.8\,M_\odot$	$1996\,M_\odot$
$6.3\,h^{-1}$Mpc	1728^3	3456^3	$182\,h^{-1}$pc	$5.19 \times 10^3\,M_\odot$	$1.04 \times 10^5\,M_\odot$
$11.4\,h^{-1}$Mpc	3072^3	6114^3	$186\,h^{-1}$pc	$5.47 \times 10^3\,M_\odot$	$1.10 \times 10^5\,M_\odot$
$20\,h^{-1}$Mpc	5488^3	10976^3	$182\,h^{-1}$pc	$5.19 \times 10^3\,M_\odot$	$1.04 \times 10^5\,M_\odot$
$114\,h^{-1}$Mpc	3072^3	6144^3	$1.86\,h^{-1}$kpc	$5.47 \times 10^6\,M_\odot$	$1.09 \times 10^8\,M_\odot$
$1\,h^{-1}$Gpc	3072^3	6144^3	$16.3\,h^{-1}$kpc	$3.62 \times 10^9\,M_\odot$	$7.24 \times 10^{10}\,M_\odot$
$3.2\,h^{-1}$Gpc	4000^3	8000^3	$40.0\,h^{-1}$kpc	$5.67 \times 10^{10}\,M_\odot$	$1.14 \times 10^{12}\,M_\odot$

3 Cosmological structure formation

In Figure 1 we show the matter (green) and halo (orange) distributions in a thin slice at redshift $z = 8$ from our largest, 20 Mpc/h box simulation with 5488^3 particles. The cosmic web is already well-developed and highly nonlinear at these small scales even at such an early time. At this point there are over 110 million resolved dark matter halos in the box. The larger, rare halos are strongly clustered, with a spatial distribution which is highly biased with respect to the underlying density field, and largely follows the high-density filaments and knots. However, there are a fair number of smaller halos (minihaloes) which are found in mean and low-density (void) regions. The reason for this is that at this time the smallest minihaloes become very common haloes, with $\nu = \delta_c/\sigma(M) < 1$, where $\delta_c \sim 1.69$ is the linear overdensity at collapse time predicted by the top-hat model and $\sigma(M)$ is the density field variance at the appropriate mass scale M. A number of large-scale voids, from a few to ~ 10 Mpc in size, are found in our computational volume, as well as a large number of high density peaks. The density therefore varies very significantly between sub-volumes. For example, at ~ 0.5 Mpc scale the density variation is 1 order of magnitude even at $z = 28$ and reaches $\sim$2 orders of magnitude at $z = 8$.

3.1 Halo mass function

We locate the collapsed halos on-the-fly, as the code is running, using a spherical overdensity halo finder with overdensity of 178. This is done by first interpolating the particles onto a gridded density field (at resolution twice the number of particles per dimension, as listed in Table 1). Local density peaks (with density at least 100 times the average) are located and spherical shells are expanded around each peak until the threshold overdensity is reached. The resulting object is then marked as a halo (objects with less than 20 particles are discarded as they cannot be reliably identified). The halo centre position is calculated more precisely by quadratic interpolation within the cell and the particles within the halo virial radius are identified and

[a] http://www.cita.utoronto.ca/mediawiki/index.php/CubePM

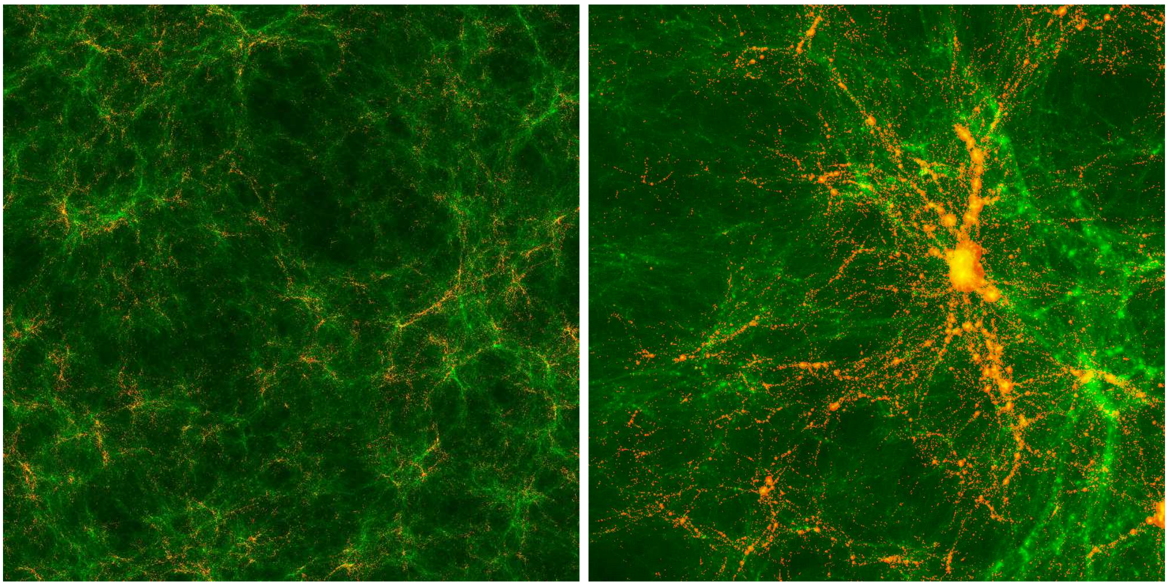

Figure 1: Cosmic Web at redshift $z = 8$ from simulation with boxsize $20\,h^{-1}$ Mpc and $5488^3 = 165$ billion particles resolving halos with minimum masses of $10^5 M_\odot$. Shown are projections of the total density (green) and halos (actual size; orange). Slice is 444 h^{-1}kpc thick, images are of the full box (left) and of a zoomed sub-region $1.8{\times}1.8$ h^{-1}Mpc in size (right).

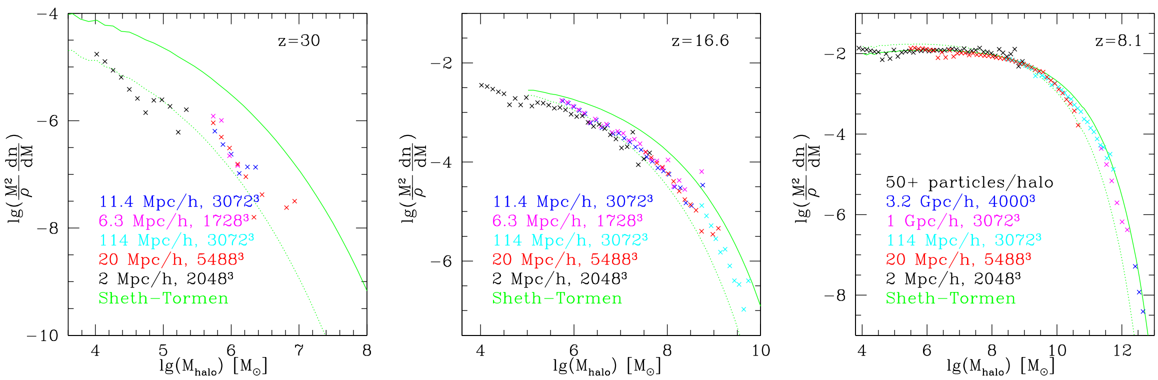

Figure 2: Halo multiplicity functions at redshifts $z = 30$ (left), $z = 16.6$ (middle) and $z = 8$ (right).

then the halo properties, e.g. mass, velocity dispersion, center-of-mass, angular momentum, radius, etc. are calculated and saved in the halo catalogue.

The resulting halo multiplicity functions, $(M^2/\bar{\rho})(dn/dM)$, at $z = 30$, 16.6 and 8.1 are shown in Figure 2. Here we conservatively only include well-resolved halos, with at least 50 (100) particles at $z = 8$ (higher redshifts). The halo mass functions show significant differences from the widely-used Sheth-Tormen (ST) approximation [3] (solid green line), particularly for rare halos. At $z = 8.1$, ST is a reasonably good fit for halos with $M_{halo} < 10^9 M_\odot$ (corresponding roughly to ν up to a few), but over-predicts the abundances of more massive halos by a significant factor of up to a few. This is consistent with previous results on the halo mass function at high-z [4,5,6]. At higher redshifts the numerical mass functions do not agree with ST by ever larger factors, over-predicting the halo abundances by up to an order of magnitude at $z = 30$. In fact, at highest redshift, the classic Press-Schechter mass function (green dotted line) is a better fit, although it somewhat underestimates the halo abundances.

3.2 Halo bias

The halo mass function is a strongly nonlinear function of the local density. Overdense regions behave locally as universe with higher mean density producing exponentially more halos. This is directly related to the bias of the halo distribution with respect to the underlying density

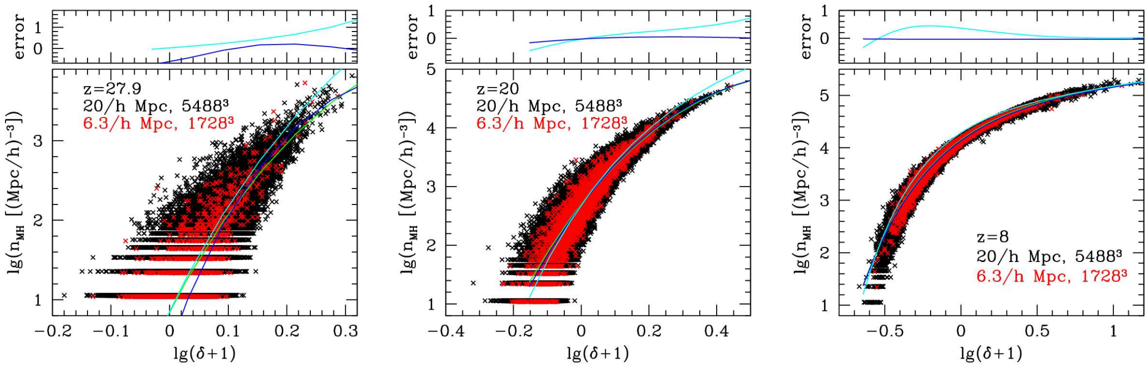

Figure 3: Number of minihaloes per unit volume vs. local overdensity, $1+\delta$, for sub-volumes of size $440\,h^{-1}$kpc at $z = 28$ (left), $z = 20$ (middle) and $z = 8$ (right). Shown are the results based on 2 simulations with same resolution, with boxsizes $6.3\,h^{-1}$Mpc (red points) and $20\,h^{-1}$Mpc (black points). Also shown are the best mean fits for $6.3h^{-1}$Mpc (dark blue line) and $20\,h^{-1}$Mpc (green line) and the extended Press-Schechter (extPS) model predictions (light blue line). Top panel shows the extPS (light blue) and $6.3\,h^{-1}$Mpc mean (dark blue) in units of the respective $20\,h^{-1}$Mpc box results.

field and is an important ingredient in many semi-analytical models of structure formation and reionization. Such models are also used as sub-grid physics in simulations when they do not have sufficient resolution to resolve all halos relevant to the questions being asked. It is therefore very important to have a handle on the correlation of mass function with local density. To this end, we use data from two of our simulations, with box sizes 20 Mpc/h, 6.3 Mpc/h. Scatter plots of the number of minihalos ($M_{halo} < 10^8 M_\odot$) vs. local density in units of the mean are shown in Figure 3. The best-fit mean relations are plotted as well. For comparison we also show an analytical bias prescription based on extended Press-Schechter theory[7]. The first observation is that results are fairly consistent between the 6.3 Mpc/h and the 20 Mpc/h runs, which have the same spatial and mass resolution, but very different volume. Both extremes, high overdensity and underdensity, are less well sampled by the smaller box, which is especially evident at high redshift, $z = 28$, but the best mean fits for each box agree with each other reasonably well. At later times, $z < 20$, they become virtually indistinguishable. The analytical model gives a relatively good prediction for the correlation at mean density and high redshift, and at high density and lower redshift, but can be off by up to a factor of 2 at other regimes. Finally, we note that there is a significant scatter in the halo number - local density relation, particularly at higher redshifts. At later times the correlation tightens, although mostly in relative terms, because the density variation range increases significantly, while the absolute value of the scatter remains roughly constant. The origins of this scatter and its effects on semi-analytical and sub-grid numerical models are currently under investigation.

Acknowledgements

We thank the Texas Advanced Computing Center for providing HPC resources and excellent support (special thanks to Bill Barth), and grants NSF AST 0708176, NASA NNX 07AH09G and NNG04G177G, and Chandra SAO TM8-9009X.

References

1. S. R. Furlanetto, S. P. Oh, and F. H. Briggs. *Physics Reports*, 433:181, 2006.
2. I. T. Iliev, P. R. Shapiro, G. Mellema, H. Merz, and U.-L. Pen. *in proceedings of TeraGrid08, ArXiv e-prints (0806.2887)*, 2008.
3. R. K. Sheth and G. Tormen. *MNRAS*, 329:61–75, 2002.
4. I. T. Iliev, G. Mellema, U.-L. Pen, H. Merz, P. R. Shapiro, and M. A. Alvarez. *MNRAS*, 369:1625–1638, 2006.
5. D. S. Reed, R. Bower, C. S. Frenk, A. Jenkins, and T. Theuns. *MNRAS*, 374:2, 2007.
6. Z. Lukić, K. Heitmann, S. Habib, S. Bashinsky, and P. M. Ricker. *ApJ*, 671:1160, 2007.
7. R. Barkana and A. Loeb. *ApJ*, 609:474, 2004.